THE JOURNAL OF BIOLOGICAL CHEMISTRY
Vol. 278, No. 30, Issue of July 25, pp. 27695–27702, 2003

Printed in U.S.A.

Recruitment of σ^{54}-RNA Polymerase to the *Pu* Promoter of *Pseudomonas putida* through Integration Host Factor-mediated Positioning Switch of α Subunit Carboxyl-terminal Domain on an UP-like Element*

Received for publication, March 25, 2003, and in revised form, May 8, 2003
Published, JBC Papers in Press, May 16, 2003, DOI 10.1074/jbc.M303031200

Raffaella Macchi, Lorena Montesissa, Katsuhiko Murakami‡§, Akira Ishihama‡, Víctor de Lorenzo¶, and Giovanni Bertoni‖

From the Dipartimento di Genetica e Biologia dei Microrganismi, Università degli Studi di Milano, via Celoria 26, 20133 Milan, Italy, the ‡Nippon Institute for Biological Science, Ome, Tokyo 198-0024, Japan, and the ¶Department of Microbial Biotechnology, Centro Nacional de Biotecnología, Consejo Superior de Investigaciones Científicas, Campus de Cantoblanco, 28049 Madrid, Spain

The interactions between the σ^{54}-containing RNA polymerase (σ^{54}-RNAP) and the region of the *Pseudomonas putida Pu* promoter spanning from the enhancer to the binding site for the integration host factor (IHF) were analyzed both by DNase I and hydroxyl radical footprinting. A short *Pu* region centered at position −104 was found to be involved in the interaction with σ^{54}-RNAP, both in the absence and in the presence of IHF protein. Deletion or scrambling of the −104 region strongly reduced promoter affinity *in vitro* and promoter activity *in vivo*, respectively. The reduction in promoter affinity coincided with the loss of IHF-mediated recruitment of the σ^{54}-RNAP *in vitro*. The experiments with oriented-α σ^{54}-RNAP derivatives containing bound chemical nuclease revealed interchangeable positioning of only one of the two α subunit carboxyl-terminal domains (αCTDs) both at the −104 region and in the surroundings of position −78. The addition of IHF resulted in perfect position symmetry of the two αCTDs. These results indicate that, in the absence of IHF, the σ^{54}-RNAP asymmetrically uses only one αCTD subunit to establish productive contacts with upstream sequences of the *Pu* promoter. In the presence of IHF-induced curvature, the closer proximity of the upstream DNA to the body of the σ^{54}-RNAP can allow the other αCTD to be engaged in and thus favor closed complex formation.

Bacterial promoters are modular DNA regions able to establish productive interactions both with subunits of RNA polymerase holoenzyme (RNAP[1]; subunit composition: $\alpha_2\beta\beta'\sigma$) and regulatory proteins (1–4). The core promoter elements are signature tags for σ factor selectivity (4). The major sigma factor σ^{70} generally directs RNAP to interact with the core DNA elements −10 and −35 (hexamers with consensus 5′-TATAAT-3′ and 5′-TTGACA-3′, respectively) (5). The core promoter elements can be both overlapped and flanked by protein-bound DNA sites involved in the fine modulation of promoter activity (2, 4). In the last decade, a considerable amount of attention has been given to a A + T-rich promoter sequence, the UP element, located upstream of the core promoter region and consisting of two distinct subsites, each of which, by itself, can be bound by the carboxyl-terminal domain of the RNAP α subunit (αCTD) (3, 6–10). αCTD recognizes and interacts with the backbone structure in the minor groove of the UP element. The A + T-rich sequence of the UP element are needed to provide the optimum width of minor groove for interaction with αCTD (7, 11). Several lines of evidence showed that the role of the UP elements is to stimulate transcription in an activator protein-independent manner and to a different extent (from 1.5 to ~90-fold) depending on the similarity with the consensus UP element sequence (3, 9). It is currently believed that the transcription stimulation by an UP element has to be traced mainly to the cooperation of the sigma factor and the α subunit in RNAP binding to the promoter (1, 12). Thus, the presence of an UP element in a promoter plays the major role of increasing the initial equilibrium constant of closed complex formation between RNAP and promoter DNA (13, 9). However, influences of α-UP element interaction on later steps in transcription initiation were also reported (13, 14). The location of the UP element with respect to the transcription start site can influence the degree of transcription stimulation (15). In the *Escherichia coli rrnB* P1 promoter, the UP element is located in a region spanning form the −40 and −60 positions and is able to increase transcription from 30- to 70-fold (6, 13). The artificial upstream re-location of the *rrnB* P1 UP element by a single turn of DNA helix decreases but does not prevent transcription stimulation, while further displacements abolish UP element-dependent transcription (15). The ability of αCTD to contact DNA and/or activator molecules at different locations upstream of the core promoter (8, 15–21) has been attributed to the flexibility of the linker connecting αCTD to the α amino-terminal domain (αNTD) (8, 22) assembled in the body of RNAP. This linker flexibility also accounts for the ability of the two copies of αCTD to function interchangeably with respect to the subsite recognition within the UP element (10). Sufficient length of the linker between αCTD and αNTD is also needed for UP element-dependent transcription activation. The linker is flexible but structured to a certain extent to facilitate the

* This work was supported by QLK3-CT-2000-00170 (MIFRIEND) Contract of the European Union. The costs of publication of this article were defrayed in part by the payment of page charges. This article must therefore be hereby marked "*advertisement*" in accordance with 18 U.S.C. Section 1734 solely to indicate this fact.

§ Present address: Rockefeller University, 1230 York Ave., New York, NY 10021.

‖ To whom correspondence should be addressed: DGBM-Università degli Studi di Milano, via Celoria 26, 20133 Milano, Italy. Tel.: 39-0250315027; Fax: 39-0250315044; E-mail: giovanni.bertoni@unimi.it.

[1] The abbreviations used are: RNAP, RNA polymerase holoenzyme; αCTD, α subunit carboxyl-terminal domains; αNTD, α amino-terminal domain; IHF, integration host factor; UAS, upstream activating sequences.

positioning of the αCTD to a proper location for interaction with the UP element (23, 15).

UP-like elements were also found in promoters recognized by alternative sigma factors, such as the σ^{D}-dependent flagellin promoter of *Bacillus subtilis* (24) and the σ^{54}-dependent *Pu* promoter of *Pseudomonas putida* (Fig. 1) (25, 26). The latter drives transcription of TOL plasmid *upper* operon for the degradation of toluene (27) and shows the typical modular structure of the σ^{54}-dependent promoters (for review, see Refs. 28 and 29) that consists of: (i) the −12/−24 region (consensus: TGGCAC N5 TTGCa/t located between positions −11 and −26) (30) recognized by σ^{54} and considered the functional analogue of −10/−35 core promoter bound by σ^{70} (31), (ii) DNA enhancer sequences (known as upstream activating sequences or UAS) targets for the activators of the σ^{54}-RNAP, usually located at >100 bp from the transcription start site, and (iii) an intervening sequence between UAS and −12/−24 motif that may contain a target site of the IHF (32), which, by its ability to bind and bend DNA sequences, assists the looping out required to bring closer together the σ^{54}-activator prebound at UAS and σ^{54}-RNAP assembled in a closed complex with −12/−24 DNA region. The productive contact between σ^{54}-activator and σ^{54}-RNAP closed complex triggers promoter opening (open complex) and eventually transcription initiation (33, 34).

Within this typical modular scheme for σ^{54}-dependent promoters, the *P. putida Pu* promoter presents unique features. In fact, our previous results showed the additional IHF role of stimulating the otherwise limiting step of closed complex formation between σ^{54}-RNAP and *Pu* DNA (26, 35). We also showed that the recognition of *Pu* promoter by σ^{54}-RNAP involves not only the −12/−24 region but also a functional equivalent of an UP element located in the intervening region, upstream to the IHF binding site. Furthermore, our data strongly suggested that the *Pu* UP element could play a key role in the IHF-mediated stimulation of closed complex formation by σ^{54}-RNAP. In this work, we closely inspected the interactions, both in the presence and absence of IHF, between σ^{54}-RNAP and the *Pu* intervening region located upstream the IHF binding site. The data strongly support the notion of a non-canonical arrangement of the stimulating DNA sequences functioning as UP element. σ^{54}-RNAP upstream interactions concentrate on two sites located in the surroundings of positions −104 and −78, respectively, thus being distant about 25 bp. In the absence of IHF and probably due to asymmetrical positioning of the upstream DNA, the two sites can be contacted interchangeably only by one αCTDs of the $\alpha_2\beta\beta'\sigma^{54}$ complex constituting the σ^{54}-RNAP. On the contrary, the bending by IHF apparently introduces symmetry to the nucleoprotein complex allowing the other αCTD to interact with the two sites. Thus, the IHF-mediated stimulation of closed complex would result from curvature-dependent increased probability of wide range upstream interactions by σ^{54}-RNAP through the αCTDs.

MATERIALS AND METHODS

Bacterial Strains, Plasmids, and General Procedures—Plasmid pEZ9 (25) contains the entire *Pu* promoter sequence as a 312-bp *Eco*RI-*Bam*HI insert in pUC18 spanning positions −208 to +93. *P. putida* strains KT2442 *hom.fg/xylRS* and its derivative HF*Pu* (*Pu*::*lacZ*, *xylR*$^+$) have been described previously (36, 37). KT2442*PuXhoCla* (*PuXhoCla*::*lacZ*, *xylR*$^+$), KT2442*PuScra1* (*PuScra1*::*lacZ*, *xylR*$^+$), and KT2442*PuScra2* (*PuScra2*::*lacZ*, *xylR*$^+$) carrying mutant *Pu*::lacZ fusions in the same location of the chromosome as HF *Pu* were obtained as follows. The *Pu* version, cloned in pUC-*PuClaI*-79, derived from pEZ9 and bearing a *Cla*I site engineered within positions −79 and −84 (26), was subjected to site-directed mutagenesis by the QuikChange™ site-directed mutagenesis kit (Stratagene) to engineer a *Xho*I site within nucleotides −121 to −126. This procedure generated the plasmid pUC-*PuClaXho*. The replacement of the 47-bp *Xho*I-*Cla*I fragment of pUC-*PuClaXho* for synthetic *Xho*I-*Cla*I fragments harboring scrambled sequences from nucleotides −105 to −120 and from −95 to −120 gave rise to plasmids pUC-*PuScra1* and pUC-*PuScra2*, respectively. The *Pu* versions present in pUC-*PuClaXho*, pUC-*PuScra1*, and pUC-*PuScra2*, respectively, were rescued as 312-bp *Eco*RI-*Bam*H fragments, fused to *lacZ* by cloning in the corresponding sites of pBK16 vector (36) and recombined with the homology fragment inserted in the chromosome of KT2442 *hom.fg/xylRS* as described previously (36). All cloned inserts and DNA fragments were verified before use by automated DNA sequencing. Recombinant DNA manipulations were carried out according to published protocols (38).

Proteins and Protein Techniques—Accumulation of β-galactosidase raised by *lacZ* fusions was measured in *P. putida* KT2442 cells permeabilized with chloroform and sodium dodecyl sulfate (SDS) as described by Miller (39) under the conditions specified in each case. Purified σ^{54} factor and IHF were kindly donated by B. Magasanik and S. Goodman, respectively; native core RNAP was purchased from Epicenter Technology. Reconstitution of RNAP carrying (*p*-bromoacetamidobenzyl)-EDTA·Fe (Fe·BABE) on β-associated α, α(Fe)β·αβ′, β′-associated α, αβ·α(Fe)β′, and simultaneously on both α subunits, α(Fe)β·α(Fe)β′, was carried out as described by Murakami *et al.* (17, 40).

DNA Binding Assays—The DNA fragments used in DNA footprinting experiments of Fig. 2 (*A* and *B*) and Fig. 5 were excised from pEZ9 as 390-bp *Eco*RI-*Pvu*II and end-labeled at their *Eco*RI sites by in-filling the overhanging ends as described below. The collection of *Pu* promoter sequences (*Pu*-126, *Pu*-114, *Pu*-105, *Pu*-85) having the same downstream end at +45 and different upstream ends at −126, −114, −105, and −85 were generated by separate PCR amplification from pEZ9 with the common reverse primer 5′-GAGAAAATACAACATTGAAGGGTCACCACT-3′ and forward primers 5′-GCTCTAGA(*Xba*I)TACAGCCAGCGTGCTGTAGA-3′, 5′-GA*AGGCCT*(*Stu*I)GCTGTAGATTTTCTCTCATAC-3′, 5′-GCTCTAGA(*Xba*I)TTTTCTCTCATACCCCCCCT-3′, 5′-GCTCTAGA(*Xba*I)TTCTTTTTTACAAAGAAAAT-3′, respectively.

For gel retardation assays, the PCR-amplified fragments described above were end-labeled with [γ-^{32}P]ATP and T4 polynucleotide kinase. Radioactive nucleotides not incorporated in DNA were removed by centrifuging briefly in small Sephadex G-25 columns. Binding reactions were performed in a total volume of 25 μl of transcription buffer containing 35 mM Tris acetate, 70 mM KAc, 5 mM $MgAc_2$, 20 mM NH_4Ac, 2 mM $CaCl_2$, 1 mM dithiothreitol, 3% glycerol, and 40 μg/ml of poly[d(I-C)]. Labeled fragments, added to the buffer at a final concentration of 5 nM, were incubated with 100 nM IHF, 60 nM core RNAP, and a 3-fold molar excess of σ^{54} factor for 25 min at 30 °C. The entire reaction volume was loaded onto non-denaturing 4% polyacrylamide gels (acrylamide:bis ratio 80:1) in 0.5× TBE buffer (45 mM Tris borate, pH 8.3, 0.1 mM EDTA, 5 mM $MgCl_2$), electrophoresed at 12 mM at 4 °C for 6 h, and dried. Bands were visualized and quantified by Typhoon 8600 variable mode imager (Amersham Biosciences) upon storage phosphor autoradiography. DNA footprinting assays were performed in a total volume of 50 μl and with similar concentrations of end-labeled fragments and proteins used in the gel mobility-shift assays. For DNase I footprinting, after preincubation of end-labeled *Pu* DNA and proteins in transcription buffer for 25 min at 30 °C, 3 ng of DNase I were added to each sample and further incubated for 3.5 min. Reactions were stopped by addition of 25 μl of STOP buffer containing 0.1 M EDTA, pH 8, 0.8% SDS, 1.6 M NH_4Ac, and 300 μg/ml sonicated salmon sperm DNA. Nucleic acids were precipitated with 175 μl of ethanol, lyophilized and directly resuspended in denaturing loading buffer (7 M urea, 0.025% bromphenol blue, and 0.025% xylene cyanol in 20 mM Tris, pH 8) prior to loading on a 7% DNA sequencing gel. A + G Maxam and Gilbert reactions (41) were carried out with the same fragments and loaded onto the gels along with the footprinting samples. For hydroxyl radical footprinting, after preincubation of end-labeled *Pu* DNA and proteins for 25 min at 30 °C in *hydroxyl radical* buffer containing 25 mM HEPES, 70 mM KAc, 5 mM $MgAc_2$, 19 mM NH_4Ac, 0.7 mM DTT, 1% glycerol, and 40 μg/ml of poly[d(I-C)], 3 μl each of $[Fe(EDTA)]^{2-}$ (125 mM $(NH_4)_2Fe(SO_4)_2{\cdot}6H_2O$, 250 mM EDTA), 28 mM ascorbate, and 0.84% hydrogen peroxide were added to the samples and then incubated for a further 5 min. Reactions were stopped by addition of 15 μl of 0.1 M thiourea and 25 μl of STOP buffer (as above), respectively. Nucleic acids were precipitated with 200 μl of ethanol and treated for separation and visualization as described above for DNase I footprinting. For DNA footprinting in the presence of (Fe·BABE)-RNAPs, after preincubation of end-labeled *Pu* DNA and proteins for 25 min at 30 °C in *hydroxyl radical* buffer, 1 μl each of 100 mM ascorbate and 0.6% hydrogen peroxide were added to the samples and then incubated for a further 15 min. Reactions were stopped by addition of 10 μl of 0.1 M thiourea and 25 μl of STOP buffer (as above), respectively. Nucleic acids were pre-

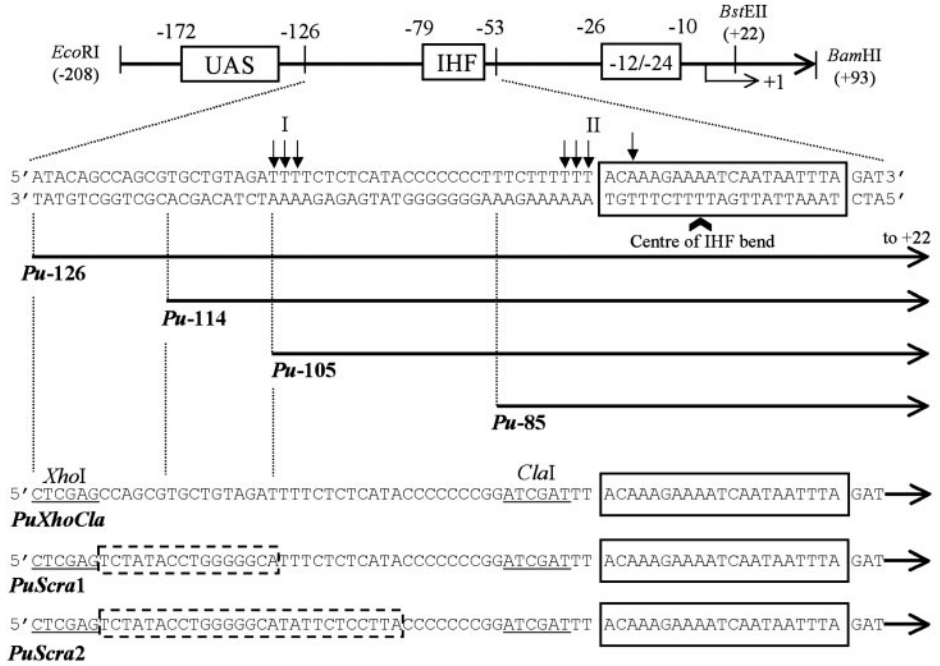

FIG. 1. **Organization of the *Pu* promoter of TOL plasmid.** The drawing at the *top* shows the 312 bp *Eco*RI-*Bam*HI insert of plasmid pEZ9 with the distribution of the functional *cis*-elements with respect to the transcription start site (+1). These include the sequence recognized by σ^{54}-RNAP (−12/−24 motif), the binding site for the IHF and the UAS, which are the target of the toluene-responsive activator of the system, XylR (46). The sequence below is an expansion of the *Pu* region spanning positions −53 to −126, including the IHF binding site (*boxed*). The *Pu* sequence regions including positions that resulted hypersensitive to hydroxyl radical cleavage (*solid arrows*) in the presence of σ^{54}-RNAP are indicated by I and II, respectively. In the text, I and II regions are referred to as UP-like$_{Pu}^{I}$ and UP-like$_{Pu}^{II}$, respectively. The predicted center of the curvature caused by IHF binding is deduced by the known crystal structure of IHF-DNA complexes (32). In the *lower part* of the figure, the configurations of the *Pu* promoter used in band-shift assays and for the functional analysis of UP-like$_{Pu}^{I}$ region *in vivo* are indicated.

cipitated with 200 μl of ethanol and treated for separation and visualization as described above for DNase I footprinting.

RESULTS

σ^{54}-RNAP Per Se Can Contact Sequence Elements Located Upstream the IHF Binding Site of Pu Promoter—The affinity of σ^{54}-RNAP for *Pu* promoter DNA lacking the sequence region located upstream the position −79 is strongly reduced (Fig. 1) (26). These data suggested that σ^{54}-RNAP could utilize *per se* additional DNA affinity elements located far upstream of the −12/−24 region involved in the interaction with σ^{54}. Since αCTD-deleted derivatives of σ^{54}-RNAP showed reduced promoter affinity (26), we also suggested that αCTD could be directly involved in the recognition of such upstream DNA, reminiscent, in this case, of the UP elements of σ^{70} promoters. Furthermore, an αCTD/UP-like interaction also seemed to be involved in the mechanism behind the stimulation of closed complex formation between *Pu* DNA and σ^{54}-RNAP on IHF binding and bending, which we referred to as IHF-mediated recruitment of σ^{54}-RNAP to the *Pu* promoter (26). To map the contact sites of σ^{54}-RNAP upstream −79 position and to reveal any possible influence of IHF-induced bending on these upstream contacts, we carried out either DNase I and hydroxyl radical footprinting assays on end-labeled DNA fragments bearing the entire *Pu* mixed with increasing amounts of σ^{54}-RNAP, both in the presence and in the absence of sub-saturating concentrations of purified IHF. As shown in Fig. 2*A* (*lanes 1–3*), the footprint of the σ^{54}-RNAP in the region spanning approximately from −83 to −108 consisted in a generalized hypersensitivity to DNase I. The addition of IHF (Fig. 2*A*, *lanes 4* and *5*) caused a further slight increase of upstream DNA reactivity to DNase I, with the exception of positions −90 and −91, appearing to be more protected from DNase I cleavage than when in the presence of σ^{54}-RNAP alone. Similar conditions of labeled *Pu* DNA/protein ratio were employed to perform hydroxyl radical footprinting assays (Fig. 2*B*). The inspection of the *Pu* DNA sequence upstream of the IHF binding site revealed both protected and hypersensitive sites in a region spanning from −95 to −109. In particular, as shown in Fig. 2*B* (*lanes 1–4*), the hydroxyl radical footprint of σ^{54}-RNAP consisted of three hypersensitive positions, −103 to −105, which seemed to be flanked by short protected regions. Apparently, the addition of IHF protein (Fig. 2*B*, *lanes 5–7*) caused minimal changes to the pattern of hydroxyl radical cutting. Examined together, these results strongly indicated that, even when unassisted, σ^{54}-RNAP can establish contacts to DNA sites located far upstream of the −12/−24 region. In the case of the hydroxyl radical footprint, the DNA region involved in interactions with σ^{54}-RNAP appeared to be limited to a short sequence in the surroundings of position −104, which we named UP-like$_{Pu}^{I}$. In our previous work (26), to explain the mechanism behind the IHF-mediated recruitment of σ^{54}-RNAP, we suggested that the distance between the −12/−24 site and the UP element(s) might disfavor either the formation or the maintenance of simultaneous binding by σ^{54}-RNAP through σ^{54} and αCTD, respectively. Thus, the key recruiting action of IHF-induced bending would have consisted of increasing σ^{54}-RNAP affinity for *Pu* DNA by bringing the −12/−24 site and the UP element(s) into a closer proximity. Apparently, from the footprinting analysis presented in Fig. 2, the ability of σ^{54}-RNAP to establish contacts with the *Pu* region located upstream of the IHF binding site seemed to be enhanced to a limited extent only by the addition of IHF. However, further analysis with free radical-delivering σ^{54}-RNAPs (see below) showed more clearly that IHF-induced bending can cause increased occupancy by αCTD of the region upstream to the IHF binding site.

The Integrity of the UP-like$_{Pu}^{I}$ Site Is Required Both for Full Promoter Affinity and IHF-mediated Recruitment of σ^{54}-RNAP—The footprinting experiments presented above allowed

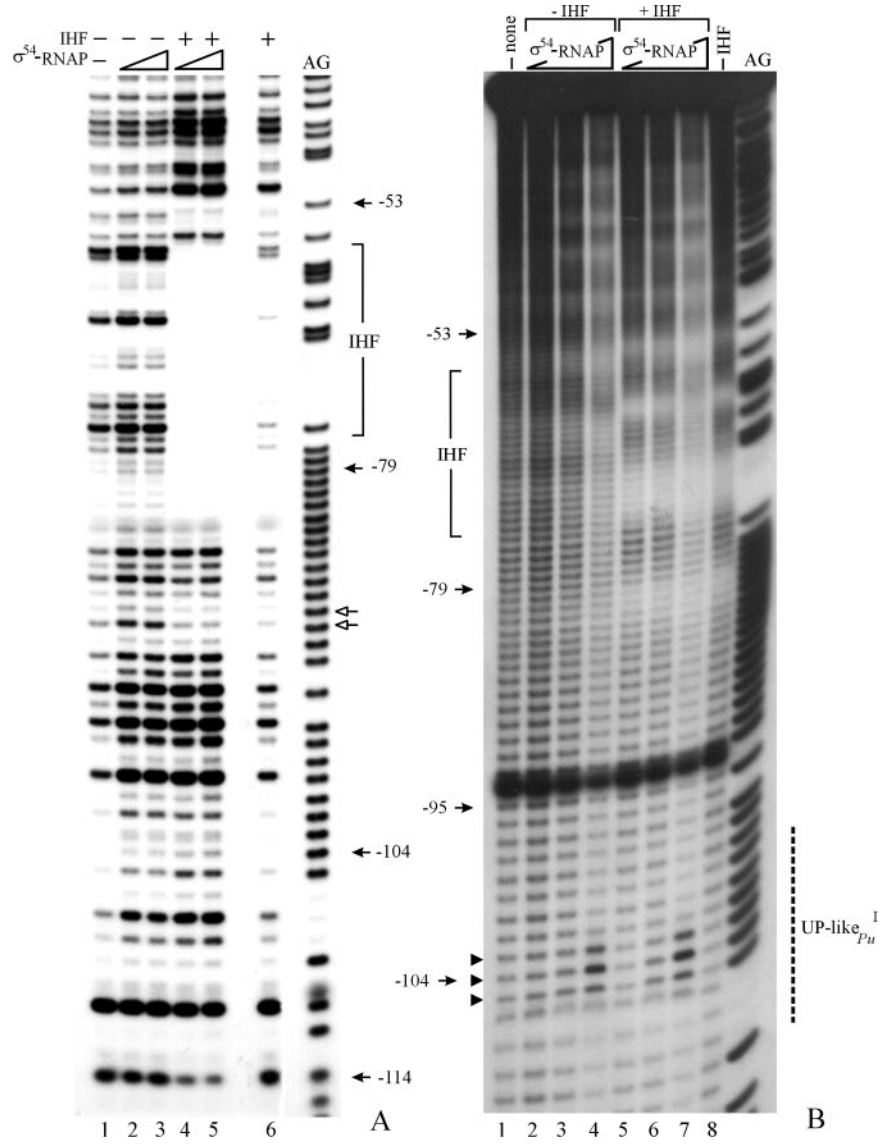

FIG. 2. **Footprinting of the *Pu* promoter with σ^{54}-RNAP and IHF.** The 390-bp *Eco*RI-*Pvu*II fragment containing the whole *Pu* promoter and end-labeled with ^{32}P at its *Eco*RI site was mixed with the proteins indicated at the top, treated with DNase I (*A*) or hydroxyl radicals (*B*), and run in sequencing gels. The A + G Maxam and Gilbert reaction of the same DNA fragment was used as a reference. The location of the IHF binding site, some coordinates along the promoter sequence, and the region corresponding to the UP-like$_{Pu}^{I}$ site are indicated to the sides. Nucleotides within the region upstream the IHF binding site which become protected to DNase I are marked with *empty arrows*. The IHF concentration was 100 nM in each case. σ^{54}-RNAP was added as core polymerase with 3-fold molar excess of purified σ^{54}. Core polymerase concentrations were 30 or 60 nM in *A* and 15, 30, or 60 nM in *B*.

us to identify an upstream DNA element, UP-like$_{Pu}^{I}$, which is contacted by σ^{54}-RNAP in the closed complex with the *Pu* promoter. To evaluate the role of the contacts with UP-like$_{Pu}^{I}$ in determining the affinity of σ^{54}-RNAP for the *Pu* promoter, we ran gel retardation assays on the nucleoprotein closed complexes formed by σ^{54}-RNAP with DNA fragments bearing either the *Pu* sequence up to position −126 (*Pu*-126; Fig. 1) supposed to include the whole UP-like$_{Pu}^{I}$ site or progressively shorter *Pu* sequences extending up to −114, −105, and −85, respectively (*Pu*-114, *Pu*-105, *Pu*-85; Fig. 1). Side-by-side comparison of the amounts of complex assembled by σ^{54}-RNAP with either *Pu*-126 or *Pu*-114, respectively, showed no significant difference (data not shown). On the contrary, the amounts of complex formed by σ^{54}-RNAP with *Pu*-105 were strongly reduced with respect to *Pu*-114 (Fig. 3, *lanes 5* and *6*). A more extended deletion up to position −85 (*Pu*-85) (Fig. 3, *lane 4*) did not decrease further the amounts of nucleoprotein complex with σ^{54}-RNAP.

To test the requirement of UP-like$_{Pu}^{I}$ integrity for the IHF-mediated recruitment of σ^{54}-RNAP, we added a sub-saturating concentration of purified IHF protein to the mixtures of σ^{54}-RNAP with *Pu*-85, *Pu*-105, and *Pu*-114, respectively. As shown in Fig. 3 (*lanes 4–9*), while the binding of σ^{54}-RNAP to *Pu*-114 could be stimulated by IHF as shown previously (26), IHF failed to enhance closed complex formation with *Pu*-105 and *Pu*-85, respectively. Thus, these results strongly indicated that the interactions established by σ^{54}-RNAP with UP-like$_{Pu}^{I}$ site in the closed complex are instrumental in determining promoter affinity. In addition, as the integrity of UP-like$_{Pu}^{I}$ is also required to observe IHF-mediated enhancement of σ^{54}-RNAP recruitment, we speculated that the promoter architecture imposed by IHF binding contributes to the interactions between σ^{54}-RNAP and the UP-like$_{Pu}^{I}$ site.

The Scrambling of UP-like$_{Pu}^{I}$ DNA Region Affects Pu Performance in Vivo—In view of the previous results *in vitro*, the disruption of the integrity of UP-like$_{Pu}^{I}$ site was expected to affect *Pu* activity. To address this issue, we aimed to monitor *in vivo* the consequences of altering the sequence spanning the UP-like$_{Pu}^{I}$ on *Pu* expression pattern. To this end, we introduced progressive sequence scrambling into the DNA region from −120 to −93 sites (Fig. 1) by replacement with synthetic double-stranded oligomers for the *wt* DNA sequence located between the *Xho*I and *Cla*I sites that were opportunely engineered within positions −126 and −121, and −84 and −79, respectively, in the *Pu* variant, *PuXhoCla* (Fig. 1). From this procedure, we obtained two *Pu* derivatives, *PuScra1* and *PuScra2* (Fig. 1), that, along with their parental *PuXhoCla*, were fused to *lacZ* and recombined into the chromosome of *P. putida* KT2442 *hom.fg/xylRS* as described previously (36). As shown in Fig. 4A, the comparison of accumulation of β-galactosidase

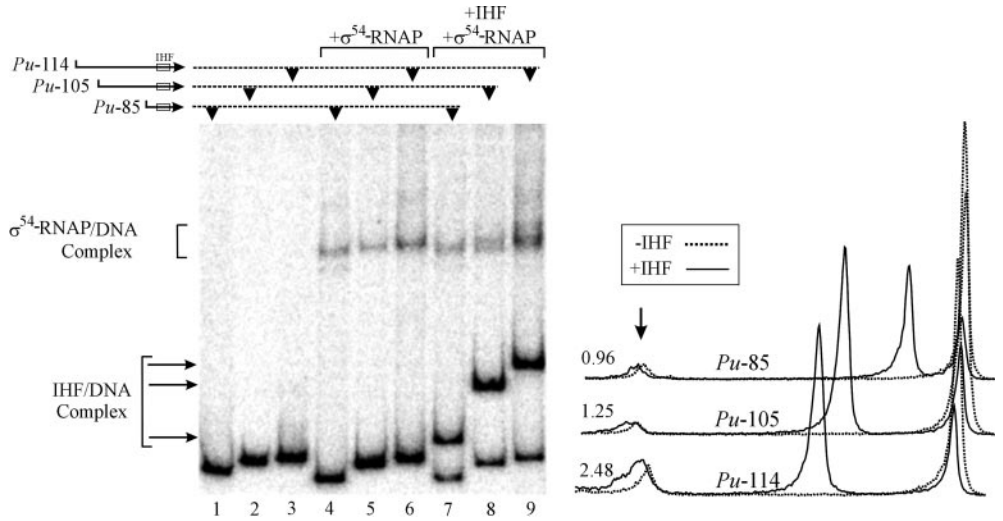

FIG. 3. **Band-shift assay of the complexes formed between *Pu* segments and σ^{54}-RNAP.** *Left*, three sequences of the *Pu* promoter spanning positions −114 to +45 (*Pu*-114), −105 to +45 (*Pu*-105), and −85 and +45 were end-labeled with ^{32}P, mixed with 60 nM σ^{54}-RNAP in the absence and in the presence of 100 nM IHF, and run in a gel retardation assay as explained under "Materials and Methods." The location of the different complexes is indicated to the sides. *Right*, superimposed profiles from scans of *lanes 4* and *7* (*Pu*-85), *5* and *8* (*Pu*-105), *6* and *9* (*Pu*-114), respectively, are shown. The *vertical arrow* indicates the position of the σ^{54}-RNAP-DNA complexes. The percentage of volume under each peak with respect to the total volume of the lane profile was calculated. The value close to the profiles of each promoter indicates the ratio between the percentage volume of the peaks corresponding to the σ^{54}-RNAP/DNA complexes in the presence and in the absence of IHF, respectively. For *Pu*-85, *Pu*-105, and *Pu*-114, the absolute percentage values of peak volumes for σ^{54}-RNAP-DNA complexes in the absence of IHF resulted 8.5, 6.4, and 13.2%, respectively.

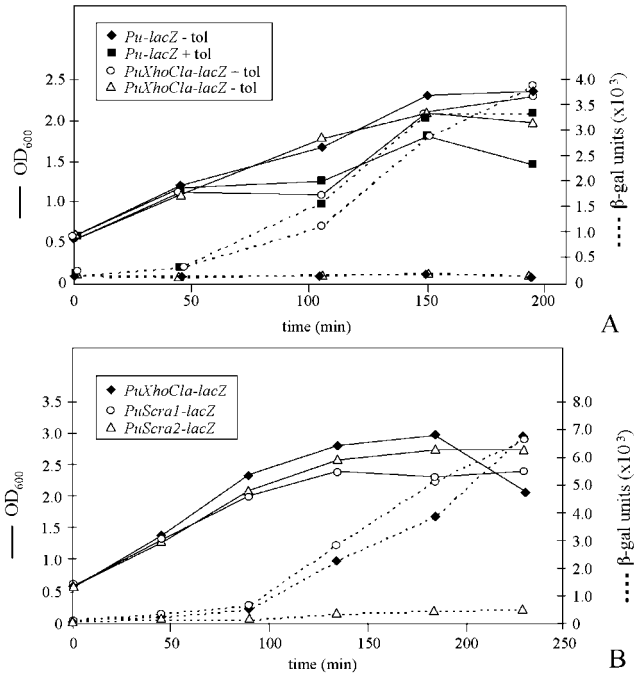

FIG. 4. **Involvement of UP-like$_{Pu}^{I}$ region in *Pu* promoter activity *in vivo*.** *P. putida* KT2442 derivatives bearing the *Pu-lacZ*, *PuXhoCla-lacZ*, *PuScra1-lacZ*, and *PuScra2-lacZ* transcriptional fusions recombined into the same site of the chromosome, respectively, were tested for the performance of expression of the *lacZ* reporter gene during the growth at 30 °C in LB medium (38). Each strain was grown until cultures had an absorbance of 0.5 at 600 nm. Toluene was then administered and the incubation continued for the subsequent 3.5 h. Accumulation of β-galactosidase along the time and growth curves of each strain after toluene addition are shown. *A*, comparison of the performances of *Pu-lacZ* and *PuXhoCla-lacZ* in the presence and in the absence of induction with toluene, respectively. *B*, comparison of the performances of *PuXhoCla-lacZ*, *PuScra1-lacZ*, and *PuScra2-lacZ*, respectively, upon toluene induction.

upon toluene induction of HF*Pu* (*Pu*::*lacZ*, *xylR*$^+$) and KT2442*PuXhoCla* (*PuXhoCla*::*lacZ*, *xylR*$^+$), respectively, revealed that the engineering of the *Xho*I and *Cla*I sites described above did not affect *Pu* performance. On the contrary, as shown in Fig. 4*B*, the comparison of β-galactosidase accumulation upon toluene induction of KT2442*PuXhoCla,* KT2442*PuScra1* (*PuScra1*::*lacZ*, *xylR*$^+$) and KT2442*PuScra2* (*PuScra2*::*lacZ*, *xylR*$^+$), respectively, revealed that the promoter activity of *PuScra2* was severely impaired. Since the sequence scrambling did not introduce either phase alteration of key regulatory sites (UAS, IHF box and −12/−24 sites) or a predictable drastic variation of promoter DNA curvature (42), we inferred that the reduction of promoter activity of *PuScra2* was caused by the destruction of upstream contacts between σ^{54}-RNAP and the UP-like$_{Pu}^{I}$ site.

Monitoring the Positioning of the Two αCTDs of σ^{54}-RNAP along Upstream Sequences of the Pu Promoter in the Absence and in the Presence of IHF—In the $\alpha_2\beta\beta'$ core RNAP complex, the two identical α subunits can be distinguished by their arrangement with respect to β and β′ subunits. In fact, one α, α^{I}, interacts with the β, whereas the other, α^{II}, interacts with β′ (43, 40, 17). To provide a more precise definition of the positioning of the αCTD of α^{I} and α^{II} (αCTD^{I} and αCTD^{II}, respectively) along the *Pu* DNA region upstream the IHF site, we set out to exploit the UP DNA cleavage capability caused by free radicals originated from (*p*-bromoacetamidobenzyl)-EDTA·Fe (Fe·BABE) attached to the UP contact surface of one or both α subunits assembled in the RNAP holoenzyme complex (40, 17). We prepared free radical-releasing σ^{54}-RNAP by adding a saturating amount of σ^{54} both to oriented-α and non-oriented (Fe·BABE)-labeled RNAP core complexes: α^{I}(Fe)/α^{II} and α^{I}/α^{II}(Fe), in which the (Fe·BABE) moiety is bound to αCTD^{I} and αCTD^{II}, respectively, and α^{I}(Fe)/α^{II}(Fe), in which the (Fe·BABE) moiety is bound to both αCTDs. Such (Fe·BABE)-labeled σ^{54}-RNAPs were incubated with end-labeled *Pu* promoter DNA, and the pattern of *Pu* DNA fragmentation was analyzed in sequencing gels as in the footprinting experiments presented in Fig. 2 (*A* and *B*). To test any differential influence of IHF on upstream DNA occupancy by αCTD^{I} or αCTD^{II}, a set of reactions was also incubated in the presence of IHF. As shown in Fig. 5, in the absence of IHF, both α^{I}(Fe)/α^{II}(Fe) and α^{I}(Fe)/α^{II} (*lanes 2* and *3*) could produce in the UP-like$_{Pu}^{I}$ region

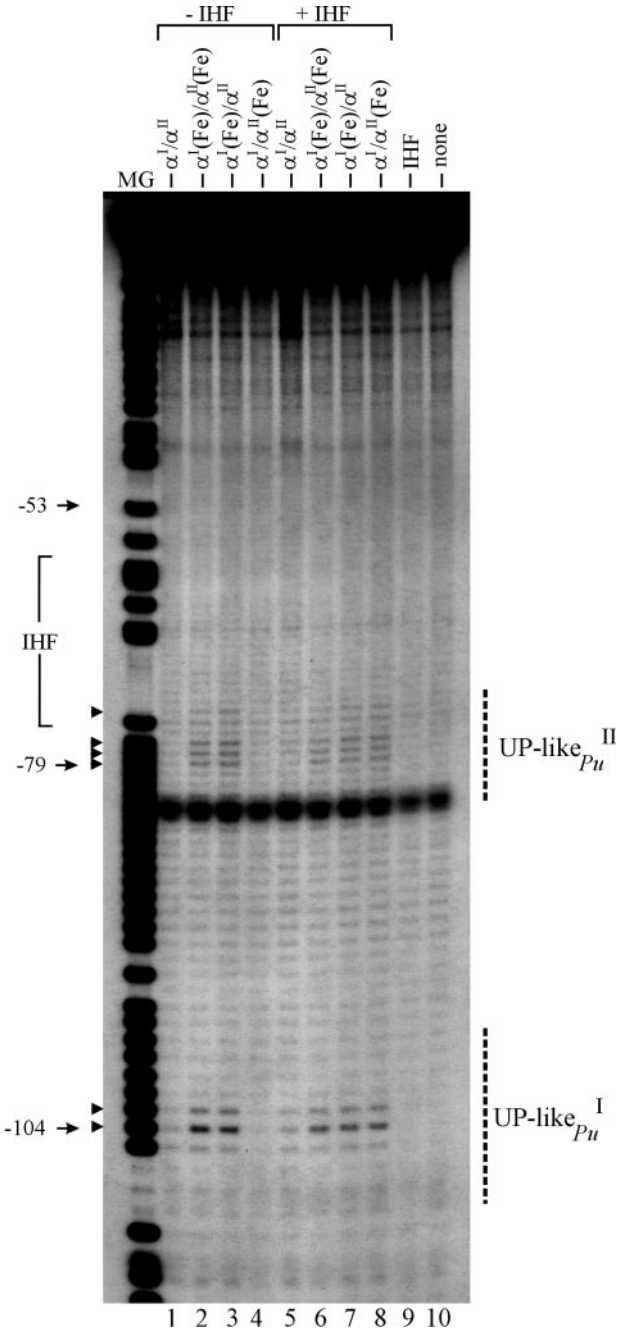

FIG. 5. **Monitoring the positioning of the two αCTDs of σ^{54}-RNAP along upstream sequences of the *Pu* promoter.** The same end-labeled fragment as Fig. 2 was incubated separately with the (Fe·BABE)-labeled σ^{54}-RNAPs indicated at the *top*, both in the presence and in the absence of IHF, and then run in a sequencing gel. No protein, IHF alone, and unlabeled σ^{54}-RNAP were used as negative controls. The location of the IHF binding site, some coordinates along the promoter sequence, and the regions corresponding to the UP-like$_{Pu}^{I}$ and UP-like$_{Pu}^{II}$ sites are indicated to the *sides*, using the Maxam and Gilbert A + G reaction as a reference. Nucleotides, which become hypersensitive to the cleavage with hydroxyl radicals, are indicated with closed arrows (see Fig. 1). The concentration of IHF used was 100 nM. RNAPs contained 60 nM, core enzyme mixed, in each case, with a 3-fold molar excess of purified σ^{54}.

a fragmentation pattern that was very similar to the hydroxyl radical hypersensitivity profile at positions −103, −104, and −105 displayed by the end-labeled *Pu* in the presence of unlabeled σ^{54}-RNAP (Fig. 2*B*, *lanes 1–4*). Furthermore, both α^{I}(Fe)/α^{II}(Fe) and α^{I}(Fe)/α^{II} could produce another discrete pattern of fragmentation closer to the IHF binding site, involving positions spanning from −74 to −79. We named this second αCTD-interacting region, which did not result so evident in the previous footprinting experiments (Fig. 2, *A* and *B*), UP-like$_{Pu}^{II}$. Unlike α^{I}(Fe)/α^{II}(Fe) and α^{I}(Fe)/α^{II}, in the absence of IHF the other oriented-α σ^{54}-RNAP, α^{I}/α^{II}(Fe), could not produce any significant fragmentation of the end-labeled *Pu* DNA (Fig. 5, *lane 4*). The addition of IHF did not substantially modify the fragmentation pattern by α^{I}(Fe)/α^{II}(Fe) and α^{I}(Fe)/α^{II}. On the contrary, the presence of IHF increased the fragmentation by α^{I}/α^{II}(Fe). In fact, under these conditions, α^{I}/α^{II}(Fe) was also able to generate a fragmentation pattern (Fig. 5, *lane 8*) identical to that of α^{I}(Fe)/α^{II}(Fe) and α^{I}(Fe)/α^{II}. Taken together, these results clearly revealed that αCTD interaction with the *Pu* upstream region can occur at two unusually distant sites, UP-like$_{Pu}^{I}$ and UP-like$_{Pu}^{II}$, respectively. Both sites can be bound interchangeably by αCTD^{I}, both in the absence and in the presence of IHF. Unlike αCTD^{I}, and probably due to an asymmetrical arrangement of the DNA upstream the IHF site, αCTD^{II} can efficiently contact both UP-like$_{Pu}^{I}$ and UP-like$_{Pu}^{II}$ only in the presence of IHF protein. These results strongly suggest that when the *Pu* promoter DNA conformation is structured by the binding and bending of IHF, the two αCTD can distribute simultaneously and interchangeably among UP-like$_{Pu}^{I}$ and UP-like$_{Pu}^{II}$.

DISCUSSION

The activity of the *Pu* promoter of *P. putida* is strongly influenced by DNA architecture. Remarkably, the bending activity of IHF strongly augments the probability of interaction between the activator XylR and σ^{54}-RNAP (44) and also positively influences the docking of σ^{54}-RNAP on the promoter (26). Our previous studies showed the involvement of αCTD in the interaction with a *Pu* region reminiscent of an UP element located upstream to the IHF binding site (26). Furthermore, our results suggested that the upstream interactions of σ^{54}-RNAP by αCTD could play an active role in its IHF-mediated recruitment. However, the relationship between topology of the promoter DNA and topography of such upstream interactions required further clarification. In fact, this might be at the basis of the IHF-mediated enhancement mechanism of closed complex formation. In this study, we investigated the nature and the role of the upstream contacts that σ^{54}-RNAP is able to establish with the *Pu* promoter both in the presence and in the absence of IHF protein. The footprinting experiments presented in Fig. 2 sustained more clearly than our previous works (26) the notion that σ^{54}-RNAP *per se* is able to establish contacts with DNA sequences located upstream to the IHF binding site. In addition, these experiments allowed us to identify a discrete upstream DNA site surrounding position −104, UP-like$_{Pu}^{I}$ (Fig. 2*B*), engaged in the interactions with σ^{54}-RNAP. Then, we addressed the issue of the functional significance of the σ^{54}-RNAP/UP-like$_{Pu}^{I}$ contacts. At least two lines of evidence indicated that the σ^{54}-RNAP contacts with UP-like$_{Pu}^{I}$ are functional interactions participating in *Pu* promoter activity. First, alterations of the *Pu* sequence spanning from −114 to −85 positions (*Pu*-105 and *Pu*-85, respectively) affect promoter affinity for σ^{54}-RNAP *per se* (Fig. 3, *lanes 4–6*). Second, the rearrangement of the sequence surrounding UP-like$_{Pu}^{I}$ in *Pu*-Scra2 derivative severely affects *Pu* activity *in vivo*. The experiment presented in Fig. 3 also indicated that UP-like$_{Pu}^{I}$ participates in the IHF-mediated stimulation of closed complex formation by σ^{54}-RNAP even though its occupancy by σ^{54}-RNAP did not seem to change significantly upon the addition of IHF (Fig. 2*B*). In our previous work (26), to explain the IHF-mediated recruitment of σ^{54}-RNAP, we considered the possibility that IHF binding and bending could strengthen the upstream contacts established by αCTD with *Pu* DNA. We figured

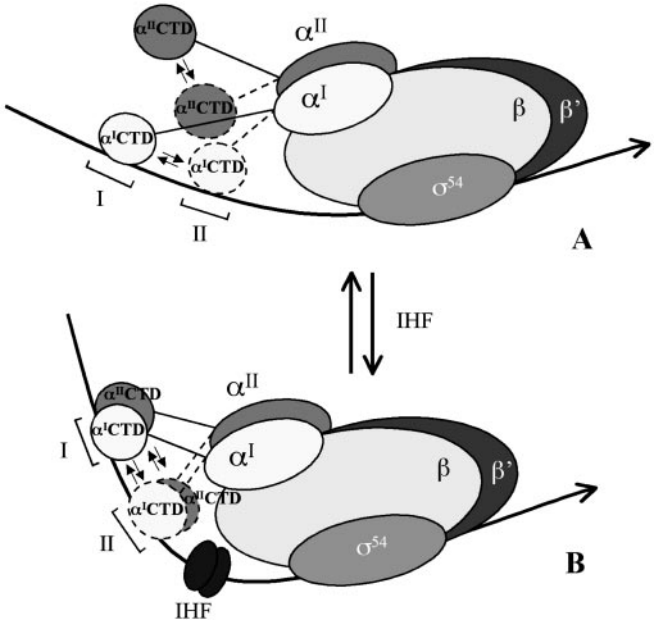

FIG. 6. **IHF-assisted positioning of the αCTDs of σ^{54}-RNAP in the *Pu* promoter.** The drawing summarizes how the DNA bending introduced by IHF favors the interchangeable positioning of the αCTD^{II} of σ^{54}-RNAP on the UP-like$_{Pu}{}^{I}$ (*I*) and UP-like$_{Pu}{}^{II}$ (*II*) subsites, thus enhancing the closed complex formation of the holoenzyme with its target sequences at −12/−24. *A*, in the absence of IHF protein, the σ^{54}-RNAP complex interacting with −12/−24 motif through the factor σ^{54} can establish upstream contacts mainly with αCTD^{I} which collocates interchangeably on either I or II site. The interactions of αCTD^{II} with the upstream DNA are probably hindered by an unfavorable distance of both I and II sites from the body of the holoenzyme. Even though the DNA/αCTD^{II} interactions are disfavored, the binding of αCTD^{I} to the upstream sites may cooperatively assist the docking of αCTD^{II} (not represented). *B*, the promoter geometry created by the IHF binding can make the distance of both I and II sites from the body of the holoenzyme more favorable for αCTD^{II}. This supposedly strengthens both the αCTD^{II} interactions with I and II sites alone and the cooperative binding of the two αCTDs. The full positioning of the two αCTDs on the upstream DNA in the presence of IHF-induced bending would enhance closed complex formation.

that this could be accomplished by one or the combination of the following two mechanisms: (i) IHF-induced curvature centered at −68 would bring into closer proximity the −12/−24 region and an UP element located upstream of the IHF binding site, thus favoring the simultaneous interaction of σ^{54}-RNAP with both sites, and (ii) the IHF binding would locally distort the double helix of DNA strengthening the αCTD/UP interaction. However, the idea that IHF could reinforce upstream contacts by αCTD contrasted with the evidence presented in Fig. 2 that IHF addition did not substantially alter the pattern of the upstream footprint of the σ^{54}-RNAP. Furthermore, this had to be reconciled with the fact that the integrity of UP-like$_{Pu}{}^{I}$ was required both to determine promoter affinity and stimulate IHF-mediated closed complex formation. The experiments with (Fe·BABE)-labeled σ^{54}-RNAPs showed that the hypothesis of the IHF-mediated strengthening of the αCTD upstream contacts was correct. However, the possible scenario (Fig. 6) can be more complex than previously thought (Ref. 26 and see above). First, αCTD can bind to UP-like$_{Pu}{}^{I}$ and also to another site, UP-like$_{Pu}{}^{II}$, located downstream. In the absence of IHF (Fig. 6*A*), only one αCTD, αCTD^{I} (*i.e.* αCTD of α that associates with β), can bind interchangeably to both UP-like$_{Pu}{}^{I}$ and UP-like$_{Pu}{}^{II}$. These asymmetrical upstream αCTD interactions determine a first level of promoter affinity. The fact that in the absence of IHF only αCTD^{I} can interact efficiently with upstream DNA could be explained by: (i) asymmetries in the $\alpha_2\beta\beta'\sigma^{54}$ complex, (ii) the axis of the upstream DNA is not in line with the body of σ^{54}-RNAP, and (iii) a combination of point i and ii. However, the binding and bending of IHF makes the αCTD interactions more symmetrical (Fig. 6*B*). In fact, in this case, the other αCTD, αCTD^{II} (*i.e.* αCTD of α that associates with β′), can also bind interchangeably to both UP-like$_{Pu}{}^{I}$ and UP-like$_{Pu}{}^{II}$. These symmetrical αCTD interactions determine a higher second level of promoter affinity which would underlie the IHF-mediated recruitment of σ^{54}-RNAP to the *Pu* promoter. The topological shift from asymmetrical to symmetrical αCTD interactions can be attributed to the IHF-induced bending that brings the −12/−24 site and the upstream DNA into closer proximity. In fact, this would favor the σ^{54}-RNAP contacts with the upstream DNA also through the αCTD^{II} domain. Despite this IHF-mediated topological switch, the flexibility of the long unstructured interdomain linker connecting αCTD to the rest of α (8, 22) might also account for the ability of σ^{54}-RNAP to contact interchangeably the UP-like$_{Pu}{}^{I}$ and UP-like$_{Pu}{}^{II}$ sites located at a distance from the −12/−24 core promoter region.

Both UP-like$_{Pu}{}^{I}$ and UP-like$_{Pu}{}^{II}$ sites may resemble the UP element subsites, each of which constitutes a binding site for αCTD (10). The certain assignment of UP-like$_{Pu}{}^{I}$ and UP-like$_{Pu}{}^{II}$ to one of the two classes, distal- or proximal-type, of UP subsite (10) cannot be deduced from this study. Moreover, it remains to be clarified whether UP-like$_{Pu}{}^{I}$ and UP-like$_{Pu}{}^{II}$ are arranged adjacently as in the UP element consensus sequence (10) or are separated by turns of DNA helix. Hypothetically, the A-tracts at positions −102 to −105 and −77 to −82 within UP-like$_{Pu}{}^{I}$ and UP-like$_{Pu}{}^{II}$ (Fig. 1), respectively, could constitute the core subsites (7, 10, 45). In view of this, we suggested that the distance between the core A-tracts is not consistent with a side-by-side arrangement as for the UP subsites in the canonical UP element (10), and there would be turns of helix between UP-like$_{Pu}$ subsites. Despite the distance between UP-like$_{Pu}{}^{I}$ and UP-like$_{Pu}{}^{II}$, it would still be possible that the binding of one αCTD to one UP-like$_{Pu}$ subsite cooperatively assists the second copy of αCTD to bind to the other UP-like$_{Pu}$ subsite. This could be accomplished by a combination of protein-protein interaction between the two αCTDs and local DNA flexibilization. The hypersensitivity to DNase I of the region upstream to the IHF binding site (Fig. 2*A*), both in the absence and in the presence of IHF, could trace the DNA bending of the UP-like$_{Pu}$ arising from the cooperative binding of the two αCTDs. We suggest that even in the absence of IHF, the binding of αCTD^{I} to one UP-like$_{Pu}$ subsite may recruit an otherwise distant αCTD^{II} to the other UP-like$_{Pu}$ subsite, and this would originate bending of the UP-like$_{Pu}$. The promoter bending introduced by IHF that renders the UP-like$_{Pu}$ region more accessible to αCTD^{II} (see above) may result in mutual and stronger cooperative binding of two the αCTDs. The slight increase in the general DNase hypersensitivity and DNase I protection of positions −90 and −91 in the presence of IHF (Fig. 2*A*, *lanes 3* and *4*) might account for the strengthening of the cooperative binding of αCTD to the UP-like$_{Pu}$ region. Since no evidence for the occupation of other sites different to UP-like$_{Pu}{}^{I}$ and UP-like$_{Pu}{}^{II}$ resulted from the assay with α^{I}(Fe)/α^{II}(Fe) σ^{54}-RNAP, we also suggest that the cooperative occupancy of the upstream DNA region involves only UP-like$_{Pu}{}^{I}$ and UP-like$_{Pu}{}^{II}$ subsites.

In summary, the evidence presented in this work strongly supports the notion of IHF-mediated topological switch that governs the occupancy of a promoter by RNAP through the curvature-mediated modulation of αCTD interactions with the upstream promoter region. It was shown previously that, by protein-protein interaction, transcription factors can direct the αCTD positioning on the upstream promoter region (17, 19). In

a novel way, the positioning of αCTD on the *Pu* promoter would be directed predominantly by the DNA architecture.

Acknowledgments—We are grateful to S. Saini, I. Cases, E. Galli, and M. Valls for inspiring discussions; to S. Goodman (University of Southern California, Los Angeles, CA) for the kind donation of IHF protein; and to F. Vidal for helpful support in band quantification.

REFERENCES

1. Busby, S., and Ebright, R. H. (1994) *Cell* **79,** 743–746
2. Gralla, J. D., and Collado-Vides, J. (1996) in *Escherichia coli* and *Salmonella* (Neidhardt, F., ed) pp. 1232–1246, American Society for Microbiology, Washington, D. C.
3. Ross, W., Aiyar, S. E., Salomon, J., and Gourse, R. L. (1998) *J. Bacteriol.* **180,** 5375–5383
4. Ishihama, A. (2000) *Annu. Rev. Microbiol.* **54,** 499–518
5. deHaseth, P. L., Zupancic, M. L., and Record, M. T., Jr. (1998) *J. Bacteriol.* **180,** 3019–3025
6. Ross, W., Gosink, K. K., Salomon, J., Igarashi, K., Zou, C., Ishihama, A., Severinov, K., and Gourse, R. L. (1993) *Science* **262,** 1407–1413
7. Ross, W., Ernst, A., and Gourse, R. L. (2001) *Genes Dev.* **15,** 491–506
8. Blatter, E. E., Ross, W., Tang, H., Gourse, R. L., and Ebright, R. H. (1994) *Cell* **78,** 889–896
9. Estrem, S. T., Gaal, T., Ross, W., and Gourse, R. L. (1998) *Proc. Natl. Acad. Sci. U. S. A.* **95,** 9761–9766
10. Estrem, S. T., Ross, W., Gaal, T., Chen, Z. W., Niu, W., Ebright, R. H., and Gourse, R. L. (1999) *Genes Dev.* **13,** 2134–2147
11. Yasuno, K., Yamazaki, T., Tanaka, Y., Kodama, T. S., Matsugami, A., Katahira, M., Ishihama, A., and Kyogoku, Y. (2001) *J. Mol. Biol.* **306,** 213–225
12. Fredrick, K., and Helmann, J. D. (1997) *Proc. Natl. Acad. Sci. U. S. A.* **94,** 4982–4987
13. Rao, L., Ross, W., Appleman, J. A., Gaal, T., Leirmo, S., Schlax, P. J., Record, M. T., Jr., and Gourse, R. L. (1994) *J. Mol. Biol.* **235,** 1421–1435
14. Strainic, M. G., Sullivan, J. J., Velevis, A., and deHaseth, P. L. (1998) *Biochemistry* **37,** 18074–18080
15. Meng, W., Belyaeva, T., Savery, N. J., Busby, S. J., Ross, W. E., Gaal, T., Gourse, R. L., and Thomas, M. S. (2001) *Nucleic Acids Res.* **29,** 4166–4178
16. Newlands, J. T., Josaitis, C. A., Ross, W., and Gourse, R. L. (1992) *Nucleic Acids Res.* **20,** 719–726
17. Murakami, K., Owens, J. T., Belyaeva, T. A., Meares, C. F., Busby, S. J., and Ishihama, A. (1997) *Proc. Natl. Acad. Sci. U. S. A.* **94,** 11274–11278
18. Belyaeva, T. A., Bown, J. A., Fujita, N., Ishihama, A., and Busby, S. J. (1996) *Nucleic Acids Res.* **24,** 2242–2251
19. Belyaeva, T. A., Rhodius, V. A., Webster, C. L., and Busby, S. J. (1998) *J. Mol. Biol.* **277,** 789–804
20. Hochschild, A., and Dove, S. L. (1998) *Cell* **92,** 597–600
21. Law, E. C., Savery, N. J., and Busby, S. J. (1999) *Biochem. J.* **337,** 415–423
22. Jeon, Y. H., Yamazaki, T., Otomo, T., Ishihama, A., and Kyogoku, Y. (1997) *J. Mol. Biol.* **267,** 953–962
23. Fujita, N., Endo, S., and Ishihama, A. (2000) *Biochemistry* **39,** 6243–6249
24. Fredrick, K., Caramori, T., Chen, Y. F., Galizzi, A., and Helmann, J. D. (1995) *Proc. Natl. Acad. Sci. U. S. A.* **92,** 2582–2586
25. de Lorenzo, V., Herrero, M., Metzke, M., and Timmis, K. N. (1991) *EMBO J.* **10,** 1159–1167
26. Bertoni, G., Fujita, N., Ishihama, A., and de Lorenzo, V. (1998) *EMBO J.* **17,** 5120–5128
27. Ramos, J. L., Marques, S., and Timmis, K. N. (1997) *Annu. Rev. Microbiol.* **51,** 341–373
28. Buck, M., Gallegos, M. T., Studholme, D. J., Guo, Y., and Gralla, J. D. (2000) *J. Bacteriol.* **182,** 4129–4136
29. Xu, H., and Hoover, T. R. (2001) *Curr. Opin. Microbiol.* **4,** 138–144
30. Merrick, M. J. (1993) *Mol. Microbiol.* **10,** 903–909
31. Buck, M., and Cannon, W. (1992) *Nature* **358,** 422–424
32. Rice, P. A., Yang, S., Mizuuchi, K., and Nash, H. A. (1996) *Cell* **87,** 1295–1306
33. Gralla, J. D. (2000) *Nat. Struct. Biol.* **7,** 530–532
34. Zhang, X., Chaney, M., Wigneshweraraj, S. R., Schumacher, J., Bordes, P., Cannon, W., and Buck, M. (2002) *Mol. Microbiol.* **45,** 895–903
35. Carmona, M., de Lorenzo, V., and Bertoni, G. (1999) *J. Biol. Chem.* **274,** 33790–33794
36. Kessler, B., de Lorenzo, V., and Timmis, K. N. (1992) *Mol. Gen. Genet.* **233,** 293–301
37. Cases, I., de Lorenzo, V., and Pérez-Martín, J. (1996) *Mol. Microbiol.* **19,** 7–17
38. Sambrook, J., and Russell, D. (2000) *Molecular Cloning: A Laboratory Manual*, Cold Spring Harbor Laboratory, Cold Spring Harbor, NY
39. Miller, J. H. (1972) *Experiments in Molecular Genetics*, Cold Spring Harbor Laboratory, Cold Spring Harbor, NY
40. Murakami, K., Kimura, M., Owens, J. T., Meares, C. F., and Ishihama, A. (1997) *Proc. Natl. Acad. Sci. U. S. A.* **94,** 1709–1714
41. Maxam, A. M., and Gilbert, W. (1980) *Methods Enzymol.* **65,** 499–560
42. Shpigelman, E. S., Trifonov, E. N., and Bolshoy, A. (1993) *Comput. Appl. Biosci.* **9,** 435–440
43. Heyduk, T., Heyduk, E., Severinov, K., Tang, H., and Ebright, R. H. (1996) *Proc. Natl. Acad. Sci. U. S. A.* **93,** 10162–10166
44. Pérez-Martín, J., Timmis, K. N., and de Lorenzo, V. (1994) *J. Biol. Chem.* **269,** 22657–22662
45. Aiyar, S. E., Gourse, R. L., and Ross, W. (1998) *Proc. Natl. Acad. Sci. U. S. A.* **95,** 14652–14657
46. Pérez-Martín, J., and de Lorenzo, V. (1996) *J. Mol. Biol.* **258,** 562–574